QUARTERLY JOURNAL OF THE ROYAL METEOROLOGICAL SOCIETY
Q. J. R. Meteorol. Soc. **135**: 914–921 (2009)
Published online 12 May 2009 in Wiley InterScience
(www.interscience.wiley.com) DOI: 10.1002/qj.423

Stable boundary layer: Parametrizations for local and larger scales

Hannu Savijärvi*
Department of Physics, University of Helsinki, Finland

ABSTRACT: Stability functions f(Ri) for a very stable boundary layer were studied by experimenting in winter Antarctic conditions with a one-dimensional (1D) numerical model and comparing with the Plateau Site tower observations. The local representations for f(Ri) produced good simulations of the temperature profiles and wind hodographs, while the standard Monin–Obukhov formulation indicated too little, and the general-circulation model (GCM)-type formulations too much, vertical mixing.

Next, idealised simulations were made for winter-night hilly northern Finland landscape with a high-resolution 2D model, using a local f(Ri) at each column. Realistic quasi-steady mesoscale katabatic flows resulted. These enhanced vertical mixing both locally and regionally. Area-averaged (i.e. regional) surface fluxes were compared with those obtained from simulations using GCM-type large-scale stability functions over flat land. New parametrizations for both local and larger scales are suggested based on the experiments. Copyright © 2009 Royal Meteorological Society

KEY WORDS stability functions; subgrid-scale fluxes; topography; katabatic flows

Received 20 August 2008; Revised 20 March 2009; Accepted 20 March 2009

1. Introduction

The atmospheric stable boundary layer (SBL) has proved to be challenging both for theories of turbulence and for the interpretation of observations. It is also problematic for atmospheric modelling at local as well as larger scales. It often shows non-stationary and intermittent behaviour in a local scale due to several mechanisms (e.g. Mahrt, 2007). It may also induce mesoscale phenomena due to surface inhomogeneities, e.g. topography-related gravity waves and drainage flows. These mesoscale phenomena and non-stationarities are not resolved by large-scale models, yet they may induce or enhance winds locally. These might then enhance vertical mixing in the area-averaged or regional sense.

The turbulent diffusion coefficient K is described in the mixing length (Blackadar, 1957) closure via

$$K = \left|\frac{\partial \mathbf{V}}{\partial z}\right| l^2 \mathrm{f}(Ri) = K_{\mathrm{neutral}} \cdot \mathrm{f}(Ri), \qquad l = \frac{\kappa z}{1 + \kappa z/\lambda} \tag{1}$$

where $\mathbf{V}$ is wind, λ asymptotic mixing length, κ the von Kármán constant, and f(Ri) a semi-empirical function of stability measured by the Richardson number Ri. In statically stable conditions $Ri > 0$ and $1 > \mathrm{f}(Ri) > 0$. Analogous stability functions are used in turbulent kinetic energy (TKE) closures and in surface fluxes, e.g. for the transfer coefficients $C = C_{\mathrm{neutral}} \cdot \mathrm{f}(Ri)$. The standard Monin–Obukhov (M–O) theory for stable, homogeneous and stationary conditions leads to a critical Ri (Ri_{c}) of about 0.20, beyond which the turbulence should vanish. However, many theories, laboratory experiments and observations point to weak turbulence beyond $Ri = 0.2$ even in the local scale (here: 1–2 km around the site), which results in a 'short-tail' type of f(Ri) without Ri_{c} (King *et al.*, 2001).

In atmospheric models, vanishing of K beyond Ri_{c} tends to lead to problems. Therefore even in high-resolution models some kind of small background turbulence is often applied (e.g. f(Ri) is set to 0.05 for large Ri). In larger-scale numerical weather prediction (NWP) and climate models (GCM) f(Ri) has to be enhanced much more, simply because such a 'long-tail' f(Ri) improves operational verification scores and prevents excessive cooling over land points, as has been found again and again e.g. in the European Centre for Medium-range Weather Forecasts (ECMWF) (Louis, 1979; Beljaars, 1995; Bechtold *et al.*, 2008). However, validation against local measurements then tends to show too strong mixing in the SBL, especially in areas with little subgrid-scale topographic variation, e.g. in the Met Office (UKMO) and ECMWF models over the oceans (Brown *et al.*, 2005) or in the interior of Antarctica in winter (King and Connolley, 1997). If a 'short-tail' f(Ri) is applied instead over these flat regions, the results improve (King *et al.*, 2001; Brown *et al.*, 2008). Moreover, in McCabe and Brown (2007) area averaging of surface fluxes at 1 km model resolution indicated only a little areal enhancement over southern England during

*Correspondence to: Hannu Savijärvi, Department of Physics, PO Box 64 (Gustav Hällströmin katu 2), 00014 University of Helsinki, Helsinki, Finland. E-mail: hannu.savijarvi@helsinki.fi

Copyright © 2009 Royal Meteorological Society

stable conditions, while over the more undulating northern England hills (Pennines) the area-averaged fluxes were more enhanced.

The strongly stable near-surface regimes (here: $Ri > 0.15$) are characterised by weak or no basic flow and cold (typically clear night-time) conditions with a surface inversion. In such conditions katabatic drainage winds tend to exist around local hills. These are known to develop quickly, e.g. in northern Finland over even very small slope angles ($<0.1^\circ$). In flat topography they are absent. One could therefore test the many suggested local formulations for f(Ri) by comparing the observations made in very stable conditions in a flat environment with one-dimensional (1D) model simulations. In section 2 some forms for f(Ri) are presented, and in section 3 these are applied locally on Antarctica. The set-up and the results resemble those of the idealised GABLS1 experiments (Cuxart *et al.*, 2006; Holtslag, 2006), but here the verification is made against real observations and the model includes interacting state-of-the-art radiation and ground heat diffusion schemes.

A local representation of f(Ri) is then used in each local grid column of a high-resolution two-dimensional mesoscale model with and without hills. In very stable conditions (here: clear, calm winter nights in northern Finland) quasi-stationary drainage flows develop down local hills. The area averages of the surface fluxes and of the wind and temperature profiles are calculated over the hilly area and compared to those obtained without hills in otherwise identical simulations. The area-averaged 2D results, discussed in sections 4–5, confirm that a large part of the empirical enhancement in the 'long-tail' f(Ri) arises because of the effects of the local drainage flows, and so should depend on the subgrid-scale topographic variance as found by McCabe and Brown (2007).

Because the subgrid-scale thermal katabatic flows typical at high Ri act as extra turbulence near the surface, a large-scale parametrization of f(Ri) is suggested in section 5 (based on many 2D experiments) by letting the 'long tail' of high Ri be simply a constant ('background turbulence'), the level of which depends on the subgrid-scale topographic variability, e.g. the typical hill height or the subgrid-scale topographic standard deviation. This automatically returns the 'short-tail' formulation over oceans and e.g. over the flat interior of Antarctica.

We note finally that the new parametrizations should be tested in 3D GCM and NWP environments, and that they leave plenty of scope for e.g. the more mechanical gravity wave, non-stationarity, and form-drag aspects of the SBL flows. Fortunately there are schemes and active research in these fields.

2. Stable boundary layer: Parametrizations for f_m and f_h

We thus take a pragmatic approach by experimenting in extremely stable conditions with a high-resolution 1D model (Savijärvi, 2006) and comparing the model-produced profiles with the observed profiles of wind and temperature, as in Cerni and Parish (1984). The observations are from the flat and smooth Antarctica high plateau. The model is forced by constant geostrophic wind and includes the standard Blackadar closure (1) for turbulence ($\lambda = 150$ m) plus a narrowband long-wave radiation scheme (67 bands), which has been validated against line-by-line calculations in Savijärvi (2006). In the snowy ground an optimised five-layer thermal diffusion scheme (Savijärvi, 1992) is applied, forced interactively by the evolving net energy flux at the surface.

In the very stable conditions typical of the Antarctic winter, the stability functions for momentum and heat $f_m(Ri)$, $f_h(Ri)$ become critically important for any turbulence scheme. Here $Ri = (g/\theta)\Delta\theta\Delta z/(\Delta \mathbf{V})^2$ is the bulk Richardson number across any air layer Δz, and local scaling (Nieuwstadt, 1984) is applied. Unfortunately these functions are not well known. They can be related to the standard Monin–Obukhov similarity ϕ-functions (Garratt, 1992; King and Connolley, 1997), producing the M–O scheme: $f(Ri) = (1 - 5Ri)^2$, $0 < Ri < 0.2$; $f(Ri) = 0$, $Ri > 0.2$ (the same for momentum and heat). However, beyond the indicated critical value of $Ri_c = 0.20$ the turbulent fluxes are forced to zero which is problematic for models, leading e.g. to unrealistically large surface cooling rates, so theories now tend to avoid the critical Richardson number. We test here the suggestion of Zilitinkevich *et al.* (2002, ZPK02): $f_m(Ri) = (1 + cRi + c^2Ri^2)^{-2}$, which is based on the asymptotic theory, and assume $f_h = f_m$. Taking the parameter values as applied for the Halley station data in ZPK02, constant c is about 6. In another 'short-tail' -type formulation ('$f_{sharp}(Ri)$': King *et al.*, 2001; Brown *et al.*, 2008), the M–O scheme is replaced by $(0.05/Ri)^2$ for $Ri > 0.1$.

On the observational forefront, Beljaars and Holtslag (1991, BH91) have derived purely empirical local functions $\phi(z/L)$ which are widely adopted, fit the midlatitude as well as Arctic sea-ice data (Grachev *et al.*, 2008) quite well, and which do not imply a critical Richardson number. Delage (1997, D97) developed an iterative method (applied here), which produces values for $f_m(Ri)$ and $f_h(Ri)$ from the rather complex BH91 ϕ–functions. As iteration is awkward in operational models, D97 suggested a simple approximation: $f_m(Ri) = (1 + 12Ri)^{-2}$. These 'local' suggestions for $f_m(Ri)$ and $f_h(Ri)$ are plotted in Figure 1. They produce rather similar values in slightly stable conditions ($0 < Ri < 0.1$) where the M–O theory is well established, except D97, which clearly underestimates in this region. For $Ri > 0.2$, all forms except M–O predict small but non-zero residual values and hence no critical Richardson number.

In testing with the ZPK02 scheme it was found that its slight modification

$$f_{\text{local}}\ (Ri) = (1 + 5 \cdot Ri + 44 \cdot Ri^2)^{-2} \qquad (2)$$

matched the BH91-iterated values for both f_m and f_h within ± 0.022 for all $Ri > 0$. The linear term of (2) guarantees standard M–O results for slightly stable layers

Copyright © 2009 Royal Meteorological Society

DOI: 10.1002/qj

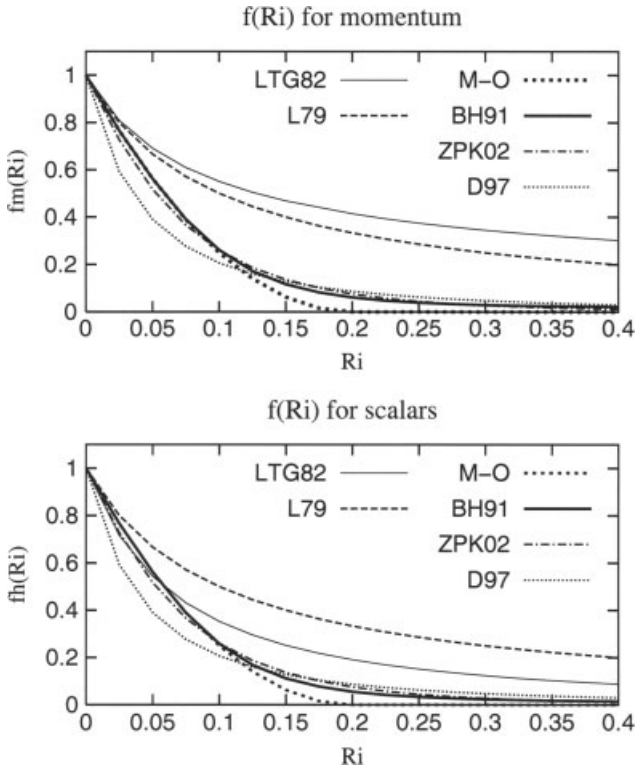

Figure 1. Some suggested analytic stability functions for momentum and scalars as functions of the bulk Richardson number *Ri*. The references are defined in the text.

($(1 + 5Ri)^{-1} \sim 1 - 5Ri$ for small Ri), while the second-order term (from the asymptotic theory) forces high-Ri values toward BH91. Equation (2) fits the BH91 values in Figure 1 within the line width, so the curve BH91 represents also (2) in Figure 1.

The above stability functions are based on local theory or local observations in a flat and homogeneous environment. The large grid squares applied in NWP and especially in climate modelling may however include considerable subgrid-scale heterogeneities, which may lead to increased regional mixing. Louis (1979) therefore suggested a widely adopted empirical 'GCM' scheme for stable conditions (L79): $f_{m,h}(Ri) = (1 + 10 \cdot Ri)^{-1}$, and Louis *et al.* (1982), more complex analytic forms (LTG82). These have been used in many NWP models (e.g. ECMWF and HIRLAM (High Resolution Limited-Area Model)) and in many climate models. These two GCM 'long-tail' schemes are also shown in Figure 1. They indicate a stronger vertical mixing than that obtained from local measurements. The newer LTG82 formulations display enhanced mixing of momentum but damped mixing of heat and scalars relative to L79.

3. Local 1D results for the Antarctic High Plateau

We now apply these functions in modelling what King and Turner (1997, p 294) called '... probably the most strongly stably stratified boundary layer observed anywhere on Earth'. They displayed mean wind hodographs and temperature profiles (shown in Figures 2–4) in the categories 'extremely stable', 'very stable' and 'stable', measured during a winter 1967 campaign at the Plateau Station, Antarctica (79.2°S, 40.5°E, 3624 m above sea level), with sensor heights 0.5, 1, 2, 4, 8, 12, 16, 20, 24, 28 and 32 m above the snow surface. The winds at the 0.5 m height were 1.5–3 m s^{-1}, so the strong stabilities (high Ri) are produced mainly by the indicated extremely cold inversion conditions. An Ekman spiral -like SBL wind structure is clearly evident in the 0.5–32 m wind hodographs with free-atmosphere wind speeds of roughly 5, 7.5 and 10 m s^{-1} associated with the three stability categories, respectively. The local environment around the Plateau Station is flat, smooth and homogeneous.

The 25-layer high-resolution 1D model uses here the observation heights at 0.5–32 m. The model was initialised via a mean mid-tropospheric winter temperature and moisture profile for the Plateau Station site (from ECMWF Re-Analysis (ERA-40) analyses) extended linearly to the surface, and was forced by a constant geostrophic wind of 5, 7.5 and 10 m s^{-1}. The ground parameters were appropriate for snow (e.g. $z_{0m} = z_{0h} =$ 0.5 mm). The net long-wave cooling of the surface together with turbulence led to a strong and quasi-steady surface inversion in about 24 hours, as in Cerni and Parish (1984). A small background value of 0.003 proved necessary for all f(Ri) to prevent numerical instabilities in the free atmosphere. The long-wave cooling within the very cold and dry air was weak (and in fact turned to weak heating in the lowest metre due to the snow surface being colder than air at 2 m, cf. Savijärvi, 2006), so the cooling of the air and the resulting temperature and wind profiles are mainly due to turbulence. Hence these local profiles should be very sensitive to the formulation of f(Ri) used in the model.

Figure 2 shows the observed profiles and 24 h model results using L79 for f(Ri). The model profiles indicate too much vertical mixing: the wind hodographs are flat, the near-surface winds are too strong and the surface and near-surface temperatures are too warm. King and Connolley (1997) found indications that the UKMO GCM, which used L79, overpredicted the wintertime surface heat flux and vertical mixing in the flat and homogeneous interior of Antarctica, where subgrid-scale effects are small. HIRLAM, which uses LTG82, tends to underpredict the cold surface and 2 m temperatures in northern Finland during inversion conditions. Savijärvi and Kauhanen (2002) showed that too strong mixing near the surface may be one of the reasons for this.

Figure 3 displays the profiles when the standard Monin–Obukhov formulation for f(Ri) is applied in the model. The model profiles are not too bad in the upper part of the SBL, but below about 10 m height they indicate too weak winds and too cold temperatures in the extremely stable and very stable cases. Hence there is presumably too little downward mixing of the warmer, windier air aloft. The associated values of the local Ri are around 0.15–0.25. As seen from Figure 1, this is where the values of the M–O f(Ri) deviate most downward from the other forms of local f(Ri), and are perhaps too low.

Copyright © 2009 Royal Meteorological Society

DOI: 10.1002/qj

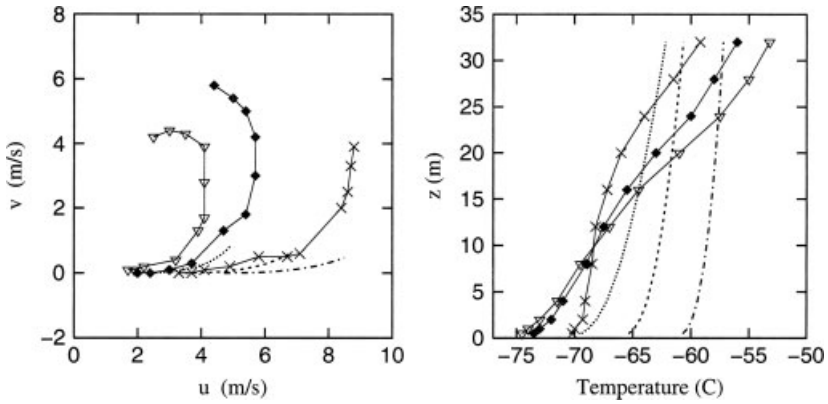

Figure 2. Observed mean wind hodographs and temperature profiles (0.5–32 m) at the Plateau Station, Antarctica, in the categories 'extremely stable' (inverted triangles), 'very stable' (diamonds) and 'stable' (crosses; data from King and Turner, 1997), and from 1D +24 h simulations with geostrophic wind speed of 5 m s^{-1} (dotted line), 7.5 m s^{-1} (dashed line) and 10 m s^{-1} (dot-dashed line), using the formulation L79 for f(Ri) in the model.

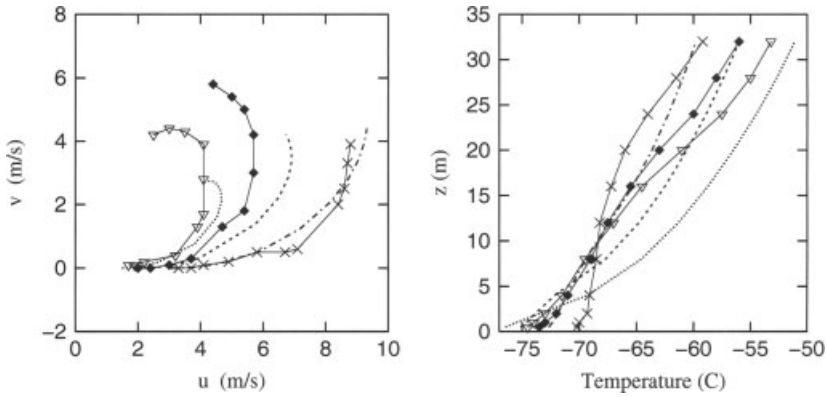

Figure 3. As Figure 2 but using the standard Monin–Obukhov formulation for f(Ri) in the model.

Figure 4 shows the 1D model results using (2). Here the match with the observed temperatures is quite good for all three stability categories. Also, the model-produced winds are fairly good, although the turning of the wind with height is less than that observed in the upper SBL (this may be due to advection which is neglected in the 1D simulations). The forms BH91 and ZPK02, being quite close to (2) (Figure 1), lead to profiles practically identical to those in Figure 4.

Finally we note that if a higher value for background turbulence than 0.003 is applied (in any of the schemes), the model profiles drift slowly toward the well-mixed conditions of Figure 2. Thus the asymptotic high-Ri limits for local f_m and f_h predicted by some theories must be very small indeed, if they exist at all in flat, smooth and homogeneous conditions.

In conclusion, it appears that a very stable boundary layer can be simulated reasonably well at the local scale by a high-resolution 1D model (equipped with good radiation and soil schemes), provided that such 'short-tail' stability functions for turbulence and for the surface interactions are used which at high Ri behave according

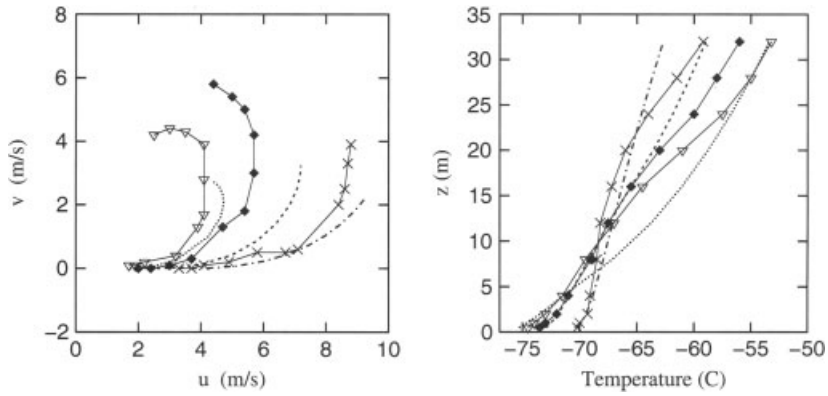

Figure 4. As Figure 2 but using Equation (2) for f(Ri) in the model.

Copyright © 2009 Royal Meteorological Society

DOI: 10.1002/qj

to the local suggestions (BH91, ZPK02, f_{sharp}, (2)). In the slightly stable midlatitude night-time conditions even the standard M–O formulation appears to work well, especially if it is site-tuned, as e.g. in Steeneveld *et al.* (2006).

4. 2D simulations over a hilly area

Experiments are now extended to variable idealised topography by applying the University of Helsinki (UH) 2D model in midwinter conditions over northern Finland, where the typical landscape consists of gently rolling forested hills. The hilltops are roughly 30–40 km apart with heights $h = 50$–100 m above the valley basins. Weak downslope flows are common during calm, clear winter nights, filling the snowy valley floors with cold stagnant air (e.g. Seppälä, 2002).

The UH sigma coordinate model (here with 4 km horizontal grid length and 25 levels up to 4 km) was set up at 67°N with two 100 m high cosine-wave hills 32 km apart in the middle of a 65-gridpoint otherwise flat area (Figure 5). The turbulence and snow schemes are the same as in the 1D simulations of section 3, with (2) used at each local column. For rapidity, a 6-band long-wave scheme was applied, based on the former ECMWF scheme, modified for high vertical resolution by Savijärvi and Räisänen (1998). The UH 2D model has been used to study many surface-driven mesoscale phenomena (for a list see Savijärvi *et al.*, 2005). For instance, it has produced the mesoscale sensible heat flux field quite well over northern Finland (compared to detailed aircraft observations) when the local topography, roughness, albedo, vegetation type etc. were defined at each grid point from maps (Savijärvi and Amnell, 2002).

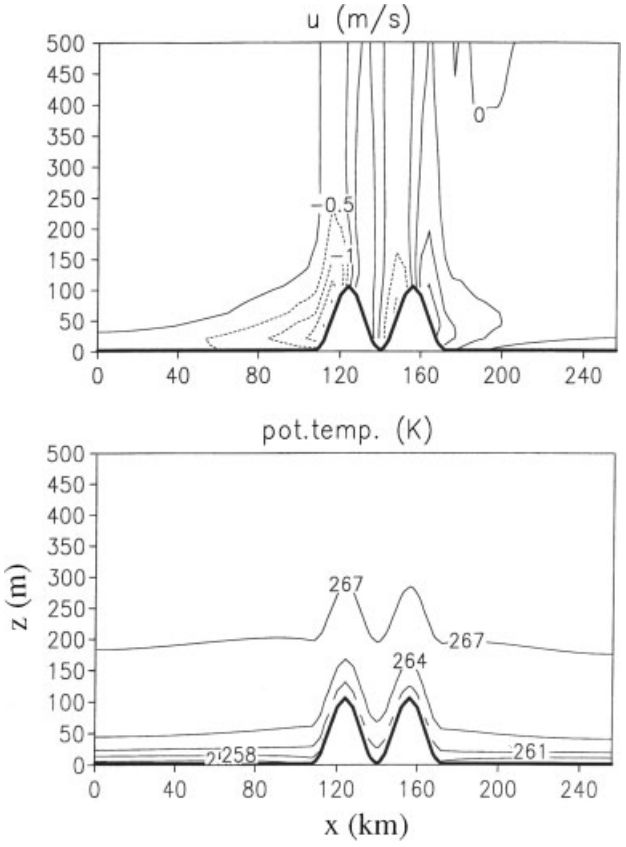

Figure 5. Cross-sections of u (plotting interval 0.5 m s^{-1}) and θ (plotting interval 3 K) in a 2D 6 h simulation over 100 m high, 32 km wide hills in typical northern Finland winter night conditions. Weak geostrophic wind is into the figure plane ($v_g = 2$ m s^{-1}). Note the katabatic mesoscale winds down the hill slopes.

The model is started from a typical midwinter midnight temperature profile for northern Finland. The ground is snowy but forested (roughness lengths $z_{0m} = z_{0h} = 50$ cm) and there are no clouds. The prevailing geostrophic wind speed $\mathbf{V}_g$ is constant in time and space, but its value varies from case to case. This leads to variable stabilities in the boundary layer, as in section 3. In the absence of solar radiation and clouds the ground rapidly cools into a quasi-steady state with a typical winter inversion developing in about six hours. Over the slopes, katabatic flows emerge. As an example, Figure 5 shows the across-hills wind component u and the potential temperature θ at 6 h for weak $\mathbf{V}_g$ directed into the figure plane ($v_g = +2$ m s^{-1}). Over the plateaus a weak and shallow cross-isobar Ekman component (negative u due to friction) can be seen, while over the hills downslope winds of 1–1.5 m s^{-1} dominate. In the θ cross-section one can recognise a strong surface inversion, cold plateaus, warmer mid-slopes (due to the locally increased mixing by the downslope winds), cold stagnant valley floor, and horizontal temperature gradients across the hills driving the local katabatic winds. All these features are commonly observed in northern Finland in nearly calm and clear wintertime conditions. They are similar to those obtained in the valley simulations of Vosper and Brown (2008).

For $\mathbf{V}_g = 0$, downslope local winds remain the only mode of wind. If the basic flow is made moderate (from any direction), the downslope perturbations u', v' still emerge in the simulations, although the total flow is of course dominated by the basic flow in cases of stronger $\mathbf{V}_g$. Standing gravity wave signatures begin to appear when the basic flow component across the hills (u_g) exceeds about 5 m s^{-1} but then the flow is no longer strongly stable near the surface due to wind mixing.

Figure 6 shows the 6 h wind speed and temperature profiles area-averaged along the lowest sigma levels over the 80 km wide hilly section for v_g of 0.3, 2 and 4 m s^{-1}. If there are no hills ($h = 0$), the 2 m air temperatures are quite cold (<-20°C), the wind shears are strong and there is a sharp wind maximum, a 'low-level jet'. These are typical SBL features observed over flat land. With hills ($h = 100$ m) but no large-scale wind (thick dot-dashed lines), the area-averaged wind profile displays a shallow katabatic wind (about 1 m s^{-1} at 10 m height) associated with slightly warmer mean temperatures near the surface due to increased vertical mixing.

The most interesting feature of Figure 6 is, however, that in the presence of hills (thicker lines) the regional averages clearly indicate increased mixing ('flatter profiles') of both temperature and wind speed throughout the

Copyright © 2009 Royal Meteorological Society

DOI: 10.1002/qj

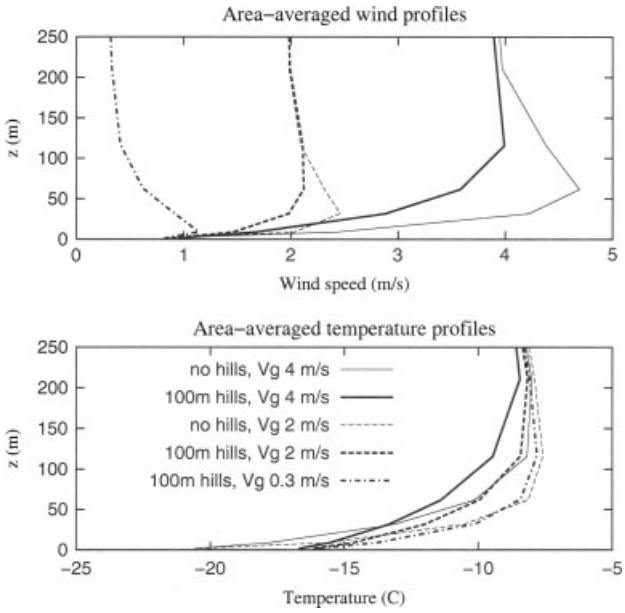

Figure 6. Wind speed and temperature profiles, area-averaged along sigma surfaces over the hilly 80 km section of Figure 5, for v_g of 0.3, 2 and 4 m s^{-1}, and either no hills ($h = 0$) or 100 m high hills in the simulation.

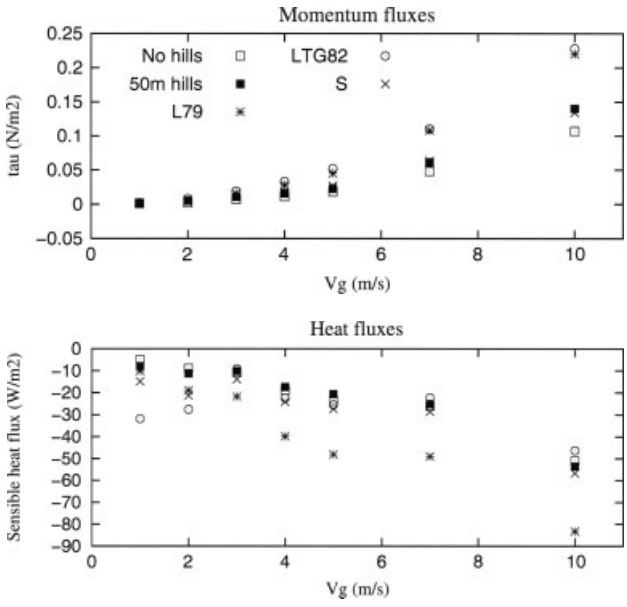

Figure 7. Area-averaged surface fluxes from the high-resolution simulations using local f(Ri), for 50 m high hills (black squares) and for no hills (white squares), as a function of the prevailing large-scale flow speed V_g. The stars, circles and crosses stand for no-hill simulations with L79, LTG82 and Equation (3) (S) used for f(Ri) respectively (GCM-type simulations).

SBL compared to the no-hill averages (thin lines). The GCM-type regional f(Ri) should therefore be applied in large-scale models not only for the surface fluxes, but throughout the SBL. Above the shallow SBL their justification disappears, however (note the same values at the 250 m height in Figure 6). Hence f(Ri) should in the free atmosphere be the local representation. This strategy has recently been adopted at ECMWF (Bechtold *et al.*, 2008), and Figure 6 supports the idea.

5. Regional f(Ri)

In the case of Figure 5, when averaged over the hilly 80 km stretch, the mean surface momentum flux amounts to 0.02 N m^{-2} and the downward heat flux 24 W m^{-2}. Over the flat regions or in a no-hill experiment, i.e. without any drainage wind contribution, the fluxes are much smaller (about 0.002 N m^{-2} and 9 W m^{-2}). One might now be tempted to estimate the regional f(Ri) by normalising the area-averaged 'hilly flux' values by the respective neutral values from a no-hill experiment, after Equation (1). There is one caveat, however. The 'neutral' values are influenced by the wind shear, but the wind shear is itself strongly controlled by stability (cf. Figures 2–4, 6). The quite strong self-correlation between wind shear and stability makes this strategy to estimate the regional f(Ri) dubious.

We therefore decided to make model experiments where the 'reference' regional surface fluxes of momentum (τ) and heat were area-averaged from high-resolution experiments, applying local f(Ri) in the SBL at each column, as above, and comparing these with no-hill fluxes using a GCM-type f(Ri) in the model. The latter case thus represents a large-scale simulation, which does not recognise any subgrid-scale topography directly and therefore tries to represent the net effect on the surface fluxes by using a long-tail f(Ri), just as a GCM or a large-grid NWP model would do.

Figure 7 shows the results for $h = 50$ m hills as the function of $\mathbf{V}_g$. The black squares are the reference regional averages for fluxes with local f(Ri) in the high-resolution model, while the open squares are the same but for no hills in the model. The difference between the black and the open squares thus displays the possible SBL flux enhancement due to topography. The stars stand for L79 and the circles for LTG82 being used for f(Ri) in the flat 'GCM-type' simulations. The crosses stand for the following simple suggestion:

$$\mathrm{f}_{\mathrm{regional}}(Ri) = \max(a,\ b) \qquad (3)$$

where a is any local 'short-tail' formulation for f(Ri), here Equation (2), and b is a tunable constant of background turbulence. The background SBL turbulence for high Ri is here thought to consist mainly of the subgrid-scale katabatic flows, which in those conditions are the main mode of near-surface wind, driving turbulence. In general the value of b should therefore depend on the properties of the subgrid-scale topography. If there are no local hills in a large grid square (e.g. in the interior of oceans or Antarctica), $b = 0.003$ and (3) returns to the local formulation (2). In Figure 7, $b = 0.05$ for momentum and 0.025 for heat and scalars. These values were found optimal for $h = 50$ m by experiment.

The relatively low 50 m hills of Figure 7 imply regional fluxes only slightly increased over the flat case values. The use of L79 or LTG82 leads in this case to a strong and systematic overestimation for momentum fluxes when

Copyright © 2009 Royal Meteorological Society

DOI: 10.1002/qj

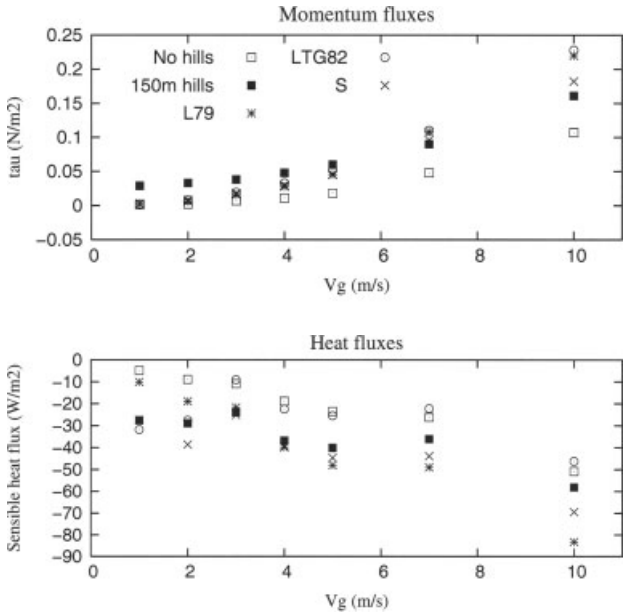

Figure 8. As Figure 7 but for hills 150 m high.

the basic flow is not weak, while (3) appears to give a good estimate for both fluxes and for all $\mathbf{V}_g$. L79 produces severe overestimates for the downward SBL heat fluxes while LTG82 overestimates them in weak wind conditions (i.e. high Ri), but underestimates instead in windy (low-Ri) conditions.

Figure 8 displays the same set-up but with higher local hills, $h = 150$ m. The stronger katabatic winds produce here a clearer impact on the regional fluxes than in Figure 7. In this case, L79 and LTG82 still overestimate the regional momentum fluxes for strong $\mathbf{V}_g$ (albeit less than in Figure 7), but underestimate for weak $\mathbf{V}_g$. The tunable (3) with $b = 0.15$ for momentum and 0.075 for scalars (crosses) is fairly close to the high-resolution reference (black squares). All parametrizations underestimate the surface stresses during low prevailing winds and high hills.

To conclude, systematic local katabatic drainage flows appear to enhance the regional downward SBL fluxes of momentum and heat, depending on the topography. In the present experiments the regional enhancements grow nearly linearly with the typical hill height h or with the subgrid-scale standard deviation of topography (zsd). The simple, tunable Equation (3) could serve as a testing vehicle for experimenting with full NWP or GCM systems. A first suggestion for the background katabatic turbulence parameter b based on the present high-resolution experiments is $b = h/1000$ m or $b = zsd/375$ m for momentum and half of that for scalars. The regional f(Ri), e.g. Equation (3) or any other 'long-tail' formulation, should be applied only in the SBL, above which b should return to a small value.

6. Conclusion

Experiments were made in the extremely stable Antarctic winter boundary layer with a column model, varying its local stability functions f(Ri) for scalars and momentum. Compared to the tower observations, fairly good results were obtained when using a local formulation without a critical Richardson number, while the standard Monin–Obukhov-based treatment resulted in too weak vertical mixing and too cold near-surface temperatures. Conversely, the GCM-type 'long-tail' formulations for f(Ri) with enhanced built-in 'regional' mixing resulted in too strong vertical mixing, and hence in too flat wind and temperature profiles. A simple local formulation for f(Ri), Equation (2), is suggested, based on the asymptotic theory.

Next, idealised winter night experiments were made for hilly northern Finland topography with a high-resolution 2D model, where the local f(Ri) formulation (2) was used at each local grid column. The model produced typical sustained downhill drainage flows which were recognizable even during weak to moderate basic wind. The area averages of the surface fluxes and the SBL wind and temperature profiles showed enhanced regional mixing (due to the steady katabatic mesoscale flows) over the hilly regions but not elsewhere.

The regional surface flux values were compared with 'GCM-type fluxes' (no explicit hills but using a GCM-type f(Ri) formulation instead in the model). The latter matched reasonably well with the high-resolution averages for moderate prevailing wind speeds and moderate hill heights but were more erroneous during low winds (i.e. high Ri) or with more extreme subgrid-scale topography (low/high hills). A tunable formulation for the regional f(Ri) is suggested (Equation (3)), where the katabatic flows are thought to promote sustained background mesoscale turbulence, described via a parameter which depends on subgrid-scale topography (e.g. the typical hill height or the standard deviation of surface topography within each grid square). This simple parametrization appeared to work reasonably well. It is open for further development.

Acknowledgements

This work was related to the Academy of Finland projects 210794 and 128799. The calculations were made in the Centre for Scientific Computing, Espoo. Comments of the three anonymous reviewers are acknowledged.

References

Bechtold P, Köhler M, Jung T, Doblas-Reyes F, Leutbecher M, Rodwell MJ, Vitart F, Balsamo G. 2008. Advances in simulating atmospheric variability with the ECMWF model: From synoptic to decadal time-scales. *Q. J. R. Meteorol. Soc.* **134**: 1337–1351.

Beljaars ACM. 1995. 'The impact of some aspects of the boundary layer scheme in the ECMWF model'. Pp 125–162 in Proceedings of Seminar on parametrization of sub-grid scale physical processes, 5–9 September 1994, ECMWF, Reading.

Beljaars ACM, Holtslag AAM. 1991. Flux parameterization over land surfaces for atmospheric models. *J. Appl. Meteorol.* **30**: 327–341.

Blackadar AK. 1957. Boundary layer wind maxima and their significance for the growth of nocturnal inversions. *Bull. Am. Meteorol. Soc.* **38**: 283–290.

Copyright © 2009 Royal Meteorological Society

DOI: 10.1002/qj

Brown AR, Beljaars ACM, Hersbach H, Hollingsworth A, Miller M, Vasiljevic D. 2005. Wind turning across the marine atmospheric boundary layer. *Q. J. R. Meteorol. Soc.* **131**: 1233–1250.

Brown AR, Beare RJ, Edwards JM, Lock AP, Keogh SJ, Milton SF, Walters DN. 2008. Upgrades to the boundary-layer scheme in the Met Office numerical weather prediction model. *Boundary-Layer Meteorol.* **128**: 117–132.

Cerni TA, Parish TR. 1984. A radiative model of the stable nocturnal boundary layer with application to the polar night. *J. Appl. Meteorol.* **23**: 1563–1572.

Cuxart J, Holtslag AAM, Beare RJ, Bazile E, Beljaars A, Cheng A, Conangla L, Ek M, Freedman F, Hamdi R, Kerstein A, Kitagawa H, Lenderink G, Lewellen D, Mailhot J, Mauritsen T, Perov V, Schayes G, Steeneveld G-J, Svensson G, Taylor P, Weng W, Wunsch S, Xu K-M. 2006. Single-column model intercomparison for a stably stratified atmospheric boundary layer. *Boundary-Layer Meteorol.* **118**: 273–303.

Delage Y. 1997. Parameterising sub-grid scale vertical transport in atmospheric models under statically stable conditions. *Boundary-Layer Meteorol.* **82**: 23–48.

Garratt JR. 1992. *The atmospheric boundary layer*. Cambridge University Press: Cambridge.

Grachev AA, Andreas EL, Fairall CW, Guest PS, Persson POG. 2008. Turbulent measurements in the stable atmospheric boundary layer during SHEBA: Ten years after. *Acta Geophysica* **56**: 142–166.

Holtslag AAM. 2006. Preface: GEWEX Atmospheric Boundary-Layer Study (GABLS) on stable boundary layers. *Boundary-Layer Meteorol.* **118**: 243–246.

King JC, Connolley WM. 1997. Validation of the surface energy balance over the Antarctic ice sheets in the U.K. Meteorological Office unified climate model. *J. Climate* **10**: 1273–1287.

King JC, Turner J. 1997. *Antarctic meteorology and climatology*. Cambridge University Press: Cambridge.

King JC, Connolley WM, Derbyshire SH. 2001. Sensitivity of modelled Antarctic climate to surface and boundary-layer flux parametrizations. *Q. J. R. Meteorol. Soc.* **127**: 779–794.

Louis J-F. 1979. A parametric model of vertical eddy fluxes in the atmosphere. *Boundary-Layer Meteorol.* **17**: 187–202.

Louis J-F, Tiedtke M, Geleyn J-F. 1982. 'A short history of the PBL parameterization at ECMWF'. pp 59–79 in Proceedings of Workshop on planetary boundary layer parameterization, 25–27 November 1981, ECMWF, Reading.

McCabe A, Brown AR. 2007. The role of surface heterogeneity in modelling the stable boundary layer. *Boundary-Layer Meteorol.* **122**: 517–534.

Mahrt L. 2007. The influence of nonstationarity on the turbulent flux-gradient relationship for stable stratification. In *Atmospheric boundary layers*, Baklanov A, Grisogono B (eds), Springer Science+Business Media: Berlin; pp 89–108. DOI: 10.1007/978-0-387-74321-9_7.

Nieuwstadt FTM. 1984. The turbulent structure of the stable, nocturnal boundary layer. *J. Atmos. Sci.* **41**: 2202–2216.

Savijärvi H. 1992. On surface temperature and moisture prediction in atmospheric models. *Contrib. Atmos. Phys.* **65**: 281–292.

Savijärvi H. 2006. Radiative and turbulent heating rates in the clear-air boundary layer. *Q. J. R. Meteorol. Soc.* **132**: 147–161.

Savijärvi H, Amnell T. 2001. Horizontal variability in the wintertime boreal boundary layer: High resolution flight observations and numerical simulations. *Theor. Appl. Climatol.* **70**: 245–252.

Savijärvi H, Kauhanen J. 2001. High resolution numerical simulations of temporal and vertical variability in the stable wintertime boreal boundary layer: A case study. *Theor. Appl. Climatol.* **70**: 97–103.

Savijärvi H, Räisänen P. 1998. Long-wave optical properties of water clouds and rain. *Tellus* **50A**: 1–11.

Savijärvi H, Niemelä S, Tisler P. 2005. Coastal winds and low-level jets: Simulations for sea gulfs. *Q. J. R. Meteorol. Soc.* **131**: 625–637.

Seppälä M. 2002. Relief control of summer wind direction and velocity: A case study from Finnish Lapland. *Norwegian J. Geography* **56**: 117–121.

Steeneveld GJ, van de Wiel BJH, Holtslag AAM. 2006. Modeling the evolution of the atmospheric boundary layer coupled to the land surface for three contrasting nights in CASES-99. *J. Atmos. Sci.* **63**: 920–935.

Vosper SB, Brown AR. 2008. Numerical simulations of sheltering in valleys: The formation of nighttime cold-air pools. *Boundary-Layer Meteorol.* **127**: 429–448.

Zilitinkevich SS, Perov VL, King JC. 2002. Near-surface turbulent fluxes in stable stratification: Calculation techniques for use in general-circulation models. *Q. J. R. Meteorol. Soc.* **128**: 1571–1587.

Copyright © 2009 Royal Meteorological Society